AIAA-2003-1275

INVESTIGATION OF A HARTMANN-SPRENGER TUBE FOR PASSIVE HEATING OF SCRAMJET INJECTANT GASES

Dustin J. Bouch
Rolling Hills Research Corporation
Torrance, CA

A. D. Cutler
The George Washington University, JIAFS
Hampton, VA

INVESTIGATION OF A HARTMANN-SPRENGER TUBE FOR PASSIVE HEATING OF SCRAMJET INJECTANT GASES

D. J. Bouch*, A. D. Cutler†
The George Washington University, JIAFS, Hampton, VA

ABSTRACT

It was postulated that heated fuel could be extracted from a Hartmann-Sprenger Tube and subsequently used as an ignition aid in a scramjet engine. Therefore, an experimental investigation of the Hartmann-Sprenger Tube was performed to gain an understanding of the geometric parameters, gas molecular weight, and flow characteristics on the gas heating performance. The Hartmann-Sprenger Tube developed for this experiment consisted of an under-expanded jet directed into a tapered, cylindrical tube. The effects of nozzle pressure, nozzle-to-tube spacing, and gas composition were explored. Also, experiments were conducted to determine the maximum amount of gas that could be extracted without significantly affecting the heating performance. Schlieren flow imagery and time traces of pressure in the tube were used to explore the major differences in heating performance at the significant modal frequencies of the apparatus. The device produced a maximum total temperature increase of a factor of approximately 2.6 in the closed configuration. Using helium as the working gas produced slightly greater heating performance (approximately 25% greater). Extracting gas from the end-wall of the apparatus decreased the end-wall to ambient temperature ratio to below a ratio of two, before one tenth of a percent of the nozzle flow was extracted.

NOMENCLATURE

a	speed of sound, m/s
f	frequency, kHz
FFT	Fast Fourier Transform
HST	Hartmann-Sprenger Tube
L	tube depth, in
P_{jet}	jet pressure, atm
P_a	ambient pressure, atm
R	jet pressure ratio, P_{jet}/P_a
R	specific gas constant, J / kg K
SLPM	Standard Liters Per Minute
T	temperature, K
T_a	ambient temperature, K
w	shock wave speed , m/s
X	nozzle-to-tube gap, in

INTRODUCTION

Motivation

The discovery of the resonance tube phenomenon, by Hartmann[1] and Sprenger[2], led to a wide variety of research and applications relating to an apparatus now commonly referred to as the Hartmann-Sprenger Tube (HST). During an experiment, Hartmann was measuring pitot pressure along the axis of an under-expanded jet and he observed at several locations that high-intensity pure-tone sound was generated. It was later understood that the tone resulted from the interaction of the jet with the cavity of the pitot probe. Although the phenomenon first observed by Hartmann was the production of high-intensity sonic waves, the majority of the subsequent related research has focused on the intense heating that occurs at the tube end-wall and corresponding large amplitude flow pulsations.

A basic HST configuration is shown in Figure 1. The concept involves an under-expanded, sonic, or supersonic jet flow impinging on a tube (closed at one end). Parameters characterizing the HST are the nozzle pressure, nozzle and tube diameters, nozzle-to-tube gap, tube length, the speed of sound inside the tube.

Three modes, each marked by the generation of varying levels of ultrasonic waves, heat, and flow pulsations, are encountered at several different combinations of the parameters previously noted. These three modes are referred to by Sarohia and Back[3] as jet-instability, jet-regurgitant, and jet-screech. The first mode, jet-instability, occurs at low nozzle jet pressures when the flow is subsonic. This mode is driven by the formation of large, periodic vortices at the nozzle exit that increase in size as they are convected downstream and result in weak compression waves within the tube. These waves, whose frequency corresponds to the nozzle vortex-shedding frequency, are not strong enough to result in a significant increase in the gas temperature.

At larger supply pressures, the nozzle produces an under-expanded jet and a periodic shock cell structure is formed between the jet and tube. Furthermore, depending upon the nozzle-to-tube gap, one of the other two modes of operation, jet-regurgitant and jet-screech results. Similar modes of operation are obtained with either a sonic or supersonic flow at the

* Graduate Research Scholar Assistant, Student Member AIAA. Rolling Hills Research Corp., Torrance, California 90505
† Associate Professor, Senior Member AIAA

nozzle exit.

Sarohia and Back explained the jet-regurgitant mode, as a periodic swallowing (inflow) and discharging (outflow) of the jet fluid at the fundamental tube resonance frequency, which can be calculated as follows:

$$f = \frac{w}{4L}$$

where w is the average-shock-wave speed, and L is the tube length. During the inflow phase, a portion of the jet flow entering the tube forms compression waves that coalesce as they travel toward the tube end-wall. These waves are then collectively reflected from the end-wall as a shock wave followed by a train of compression waves. When the wave front reaches the open end of the tube, an expansion fan is reflected into the tube causing gas in the tube to flow outward and marks the beginning of the outflow phase. Subsequently, the reflected expansion fan traverses the length of the tube and is reflected by the end-wall, towards the open end. Upon reaching the open end, the outward flow terminates and the nozzle flow reverts back to the inflow phase and marks the end of a cycle.

The generation of intense heating of the gas processed by the Hartmann-Sprenger tube coincides with the third mode of operation or jet-screech mode. This mode corresponds to a resonance phenomenon between a standing bow shock and the nozzle jet shock cell structure. It is important to note that the term jet-screech used in this work refers to a particular mode of operation for the Hartmann-Sprenger Tube. The term was originally used by Sarohia and Back after the observed the high frequency oscillation of a bow shock wave in front of the resonance tube. This mode is not related to the feedback phenomenon in under-expanded free jets discussed by Allan Powell as jet screech[4]. The latter type of jet screech occurs due to small disturbances at the nozzle exit that are convected downstream and interact with the shock cells to produce sound waves that travel upstream in the surrounding air and create disturbances at the nozzle exit, closing the loop.

During jet-screech, the nozzle jet impinging on the tube face forms a bow shock that can be set into harmonic oscillation by placing the tube face at particular locations within the shock cell structure. These locations are the compression regions of the jet or 'zones of instability' as referred to by Hartmann. An example of jet shock cell structure and the locations of the compression regions is illustrated in Figure 2. Oscillation of the bow shock in front of the tube causes strong detached shock waves to traverse the length of the tube. The bow shock wave oscillating at the opening of the tube is analogous to a leaky piston at the opening of a shock tube producing detached shock waves that traverse the length of the tube. These moving shock waves process the gas trapped inside the tube, which becomes intensely heated. Oscillation of the bow shock wave during jet-screech mode occurs at much higher frequencies than, and independent of, the tube fundamental frequency. Instead of the tube fundamental frequency, the shock wave oscillation is now dependent on the nozzle-to-tube spacing. While much progress has been made in the way of determining when and where jet-screech mode occurs, no theory exists for the mechanism.

Postulate and Objective

Since the HST is a passive device that rapidly heats the fluid, it was proposed the device be used in a scramjet engine ignition system. A schematic of a possible configuration is shown in Figure 3. The heated gas would be extracted from the tube and used as a pilot to ignite the injectant-air mixture in the combustion chamber of the engine.

As previously discussed, total temperature increases of up to a factor of approximately three[5] have been reported in Hartmann-Sprenger Tubes. The inhomogeneous ignition limit for an ambient temperature mixture of 60% hydrogen in nitrogen flowing against heated air at atmospheric pressure occurs at 928 K[6]. Assuming that similar temperatures are necessary for heated hydrogen injected into cold air and because the fuel in a scramjet engine is often used as a coolant and consequently heated above ambient conditions before injection, these findings indicate a potential for the success of an HST based ignition system. Several issues need to be investigated in order to determine the suitability of the device. Among these issues are scramjet related questions such as the minimum fuel temperature required for ignition and minimum ratio of heated to unheated fuel required for adequate piloting. These scramjet related issues are not the objective of this work and therefore not addressed here. However the HST related performance issues are.

Therefore, it is the objective of this work to: (1) ascertain the characteristics of the different modes of operation of the HST and their effect on heating performance through flow visualization, tube end-wall unsteady pressure measurement, and mean end-wall temperature measurement, (2) obtain data for a nozzle gas lighter than air to determine if greater temperatures are produced and, (3) determine the amount and temperature of gas that can be extracted from the tube.

Further details of this experiment may be found in the Master's Thesis work of Bouch[7].

METHOD

Hartmann-Sprenger Tube Design

The HST apparatus designed for this research consists of two main pieces, the convergent nozzle and the tube. The entire assembly, shown in Figure 4, is

mounted atop an optical rail that is secured to the laboratory bench.

Figure 4 shows the internal features and crucial dimensions of the HST assembly. The nozzle and tube inner dimensions were sized based on the data of Phillips and Pavli[4], where a nozzle exit diameter of 0.20-inch and tube diameter of 0.25-inch were found to produce the highest end-wall temperatures.

According to the results presented by McAlevy and Pavlak[8], tapering the resonance tube increases the heating performance of the HST. Based on this finding, as well as those by Phillips and Pavli, an HST was designed. The tube was constructed with a 6-degree taper, converging towards the closed end, and a length of 1⅞-inch.

The instrumentation port on the back side of the tube holder was sized to accommodate a ¼-inch thermocouple probe, a PCB pressure transducer probe, or a ¼-inch gas extraction line held in place with a ¼-inch Swagelock fitting.

Experimental Method

The HST performance was evaluated utilizing two distinct configurations: one to evaluate the closed tube performance (evaluation of the apparatus without extracting gas from the tube) and the other to determine the temperature and flow rate of extracted gas from the end of the tube. The HST closed-tube performance was evaluated by measuring the end-wall temperature for a range of operating pressures from 0-500 psig. The inlet pressure was measured with a 0-1000 psig Mensor gauge (±0.04% uncertainty), and the end-wall temperature was measured with a type-K thermocouple. Additionally, inlet temperature was measured with a type-T thermocouple.

In addition to temperature, the pressure at the end-wall was measured at several operating conditions, using a high frequency pressure transducer (PCB 113A, 3000 psid range, ±1% uncertainty) located at the end of the tube. A charge amplifier (PCB Mod 462A) amplified and converted the transducer output charge to a voltage signal. High frequency filtering of the voltage signal was accomplished with a signal conditioner (NEFF Instrument Corp. No. 122-123). Finally, the signal was monitored by a digital oscilloscope (HP 54522A) allowing the pressure data to be exported and saved to disk.

In the second, or "open tube", HST configuration ⅜-inch copper tubing was plumbed to the back end of the tube. A ¼-inch Swagelock T-fitting inserted into the back end of the tube holder facilitated attachment of both the tubing and a ¼-inch thermocouple probe at the tube end-wall. This allowed the flow rate of gas extracted from the back of the tube to be measured using a 0-300 SLPM flow meter (Hastings 203C, ±1% uncertainty), while simultaneously measuring the temperature.

For visualization of the flow between the nozzle and tube, a 3-inch diameter, 25-inch focal length lens Schlieren system was used. A schematic of the entire HST instrumentation system is shown in Figure 5. With the knife-edge oriented vertically, positive (increasing from left to right) density gradients produce light regions in the Schlieren images, and negative (decreasing from left to right) density gradients produce dark regions. Since the majority of the dynamic flow interaction between the nozzle and tube is the formation of shock waves with density gradients in the horizontal direction, this method was found to be effective in highlighting the shock waves.

RESULTS

Closed-Tube Performance

The first step in evaluating the HST was to determine the closed-end configuration performance. With the HST assembly in the relevant configuration a parametric experiment was performed. The nozzle pressure was varied from 0-500 psig while monitoring the end-wall temperature. This was done at a range of nozzle-to-tube gaps (X) from 0.3-inch to 1.0-inch, in order to obtain the end-wall temperature as a function of both pressure and gap.

Air Results

The end-wall temperature data as a function of pressure and X, is shown in Figures 6 and 7. Figure 6 shows the data for the small gaps and Figure 7 shows the data for the large gaps. For this investigation, the most important information to be gleaned from the data is the effect of the different modes on the temperature at the end-wall. Inspection of the data reveals the existence of multiple peaks in temperature as the pressure range is traversed. Examination of the Schlieren images of the flow between the nozzle and tube and the time-dependent pressure at the end-wall for a gap of X = 1.0-inch identifies the first (lowest pressure ratio) peak as the jet-regurgitant mode operating with the tube face inside the third shock cell from the nozzle, the second peak as the jet-regurgitant mode in the second shock cell, and the third peak as the jet-screech mode in the second shock cell.

At gaps less than 0.7-inch, the jet-regurgitant mode produces higher peak temperatures than the jet-screech mode. However, as the gap approaches 0.7-inch the jet-regurgitant temperature levels off at approximately T/T_a=1.8, whereas the jet-screech peak temperature continues to climb. The data in Figures 6 and 7 indicate a jet-screech mode trend of continually increasing peak temperature with increasing pressure. This trend is consistent with the existing HST theory (Sarohia and Back) over the range tested. The highest temperature ratio recorded in this study was T/T_a = 2.6 for R= 15.8 and X=1.0-inch. This result is in the vicinity of the maximum temperature increase of approximately 2.4 obtained by Phillips and Pavli. Although the

geometry of the present experiment was nominally the same as that of Phillips and Pavli, there were minor differences such as the location of the thermocouple. The small difference in maximum temperature is probably attributable to these differences in geometry.

In order to gain a better understanding of the flow phenomenon effects on the heating performance in the tube, an in depth investigation of the HST was conducted for the X = 1.0-inch configuration. Results of this study are shown in Figure 8. Both time-dependent pressure at the tube end-wall and Schlieren flow visualization of the nozzle-to-tube interaction were obtained. In addition to being plotted versus time, the pressure data was exported from the digital oscilloscope and transformed into the frequency domain using a Fast Fourier Transform (FFT) algorithm. The data was manipulated before performing the analysis because only 512 data points are recorded on the oscilloscope at a time. Multiplying the data by a cosine taper window eliminated the erroneous effects generated by the FFT due to a limited range of data (Bendat and Piersol[9]).

All time-dependent pressure data presented in the figure are represented on the same horizontal and vertical scales. The horizontal scale is 200 μsec per division with a sampling rate of 250 kHz and the vertical scale is 1.0 atm per division. The cases illustrated in Figure 8 correspond to the troughs and peaks of Figure 7 at X = 1.0-inch and increasing pressure ratios. Except for the final case at R = 15.8, the Schlieren images are a result of an average of multiple images taken throughout the cycle. It is important to note that the nozzle is on the right side in the image.

For R = 1.6, the nozzle pressure of the case at the top of the figure is too low to excite either of the two significant HST operating modes, jet-regurgitant or jet-screech. This is apparent in both the pressure trace and Schlieren image. The time-dependent pressure is neither periodic nor significant in magnitude indicating that none of the modes have been established. The Schlieren image shows the undisturbed jet shock cell structure due to the under-expanded nozzle flow.

The next case for R = 2.3 shows the HST operating in the jet-regurgitant mode. For this particular case, the jet-regurgitant mode occurs with the tube entrance in the third shock cell from the nozzle. The time-dependent pressure shows that a periodic waveform is created. Inspection of the FFT of the pressure data reveals a fundamental and harmonics of frequency f=2.44*N kHz, where N is 1,2,3 etc. The fundamental frequency can be estimated using:

$$f_{fund} = \frac{w}{4L} \approx \frac{a}{4L} \approx \frac{\sqrt{\gamma RT}}{4L}$$

Using the end-wall temperature of T=375 K as an estimate for the average gas temperature inside the tube and the length of the tube of L=1⅞-inch, the fundamental frequency is estimated to be $f \approx$ 2.1 kHz. The average temperature inside the tube is probably significantly lower than the end-wall temperature. However, the shock speed inside the tube is higher than the acoustic speed and these errors tend to offset each other. The calculated frequency of $f \approx$ 2.1 kHz is in the vicinity of the measured frequency of f = 2.44 kHz, indicating that the tube is excited to resonate at the fundamental. The Schlieren image shows a disturbance in the third shock cell. Furthermore, the image shows a slight expansion in the shock cell length as a function of the increasing pressure.

Additionally, it is important to notice that the fluctuating pressure waveform has the shape of a "shock-type" wave, that is characteristic of high-amplitude pressure oscillations in tubes[10], as apposed to a sinusoidal-type wave. The "shock-type" classification of the wave refers to a sharp, almost instantaneous, increase in pressure as a function of time followed by a steady drop.

The third case of Figure 8, for R = 2.7, shows data for the HST operating at a temperature minimum. The time-dependent pressure waveform is similar to the previous case for R = 2.3. However, it appears to be transitioning to a more sinusoidal shape. Furthermore, the FFT results indicate that the 1st harmonic frequency, at f = 5.1 kHz, contains as much energy as the fundamental.

The fourth case of Figure 8 for R = 4.7 shows the HST operating in the jet-regurgitant mode again. Inspection of the Schlieren image reveals that now the tube exit is inside the second shock cell from the nozzle. The jet flow is significantly disrupted by the tube interaction. The end-wall pressure waveform shows that the frequency is similar to the case for R = 2.3 where the dominant frequency was f = 2.44 kHz. Due to the resolution in the FFT, the two frequency peaks at f = 1.5 and 2.0 kHz appear to have split the energy of a frequency peak at approximately f = 1.8 kHz concealing its strength as the dominant frequency. The estimated fundamental tube frequency for this case is f = 2.3 kHz, indicating that with a dominant frequency of approximately f = 1.8 kHz, this case is probably operating at the tube fundamental frequency and therefore in the jet-regurgitant mode. Additionally, the fluctuating pressure waveform appears to have transitioned from the "shock-type" wave to a sinusoidal shaped waveform.

The fifth case of Figure 8 for R = 5.9 shows the HST operating at a temperature minimum. The time-dependent pressure waveform shows the existence of additional peaks in comparison with the previous case. Additionally, the FFT of the pressure data reveals that the overall signal strength has decreased and no clear dominating frequencies are present.

The last case of Figure 8 for R = 15.8 shows the HST operating in jet-screech mode. The pressure trace shows high frequency, periodic fluctuations in pressure. Inspecting the FFT data reveals multiple high-frequency peaks with the most significant at f = 13.7 kHz. The fluctuating pressure waveform shape for this mode is unique in comparison to the waveform shapes for the previous cases. The waveform is made up of multiple oscillations: the dominant at 13.7 kHz, and two slightly lesser in magnitude oscillations at 6.8 kHz ands 3.4 kHz. The Schlieren image shows a large bow shock wave standing off the face of the tube inside the second shock cell. The bow shock wave shows as a light, vertical band in the Schlieren image. This mode was further investigated and is subsequently discussed utilizing a sequence that illustrates its characteristics.

Examination of the fluctuating pressure traces at X = 1.0-inch for increasing pressure ratios, reveals a trend of increasing end-wall fluctuating pressure amplitude as the jet supply pressure is increased. This trend occurs until the HST is operated in the jet-screech mode. For this case, illustrated in the last image of Figure 8 for 15.8, the fluctuating pressure amplitude is lower.

Individual Mode Case Studies with Air

Schlieren images and end-wall fluctuating pressure traces were recorded at the highest temperature peaks for three nozzle-to-cavity gaps of X = 0.4, 0.7, and 1.0-inch. It is important to note that in Figures 9-12, not all pressure data is represented on the same vertical scale due to the large variation in peak-to-peak pressure of the cases studied. However, all time domain pressure data is represented on the same horizontal time scale of 200 μsec per division, with a sampling frequency of 250 kHz.

Figures 9, 10, and 12 show seven-image sequences of Schlieren images taken at equal increments within the HST cycle. Therefore, the first image, at t = 0, corresponds to the high-pressure peak of the inlet pressure cycle. The seven images represent the dynamic interaction during one complete tube inlet pressure cycle period.

Figure 9 shows the HST operating in jet-regurgitant mode at X = 0.4-inch for R = 2.1. The Schlieren images for this case represent the dynamic interaction during one tube inlet pressure cycle of 420 μs. The pressure trace shows a nearly periodic waveform. The FFT shows that the fundamental frequency is at f = 2.44 kHz. This relatively low frequency distinguishes this case as jet-regurgitant. A peak-to-peak pressure amplitude of approximately 55 psi is recorded in the pressure-time data.

The oscillating density gradient, which shows as a light, vertical band standing slightly off the face of the tube inlet, is believed to be an oscillating shock wave, similar to a bow shock wave, and indicates that the jet flow is periodically swallowed and discharged. The first two images, at t = 0 and t = 60 μs, show the jet flow in the filling phase as the shock wave moves downstream and most of the flow enters the tube. At t = 120 μs, the jet flow switches to the outflow phase. The outflow phase continues through the fifth image at t = 240 μs as the shock wave strengthens and propagates upstream towards the nozzle. The last two images, at t = 300 and t = 360 μs, show the jet flow has switched back to the inflow phase as the shock wave now moves downstream towards the tube and one cycle comes to completion.

The case in Figure 10 shows the HST operating in jet-screech mode at X = 0.7-inch for R = 10.4. There is a high-frequency pressure peak in the FFT data at f = 20.5 kHz indicative of the jet-screech mode. The Schlieren images for this case represent the dynamic interaction during one tube inlet pressure cycle of 100 μs. The image sequence illustrates the oscillating bow shock wave standing off the face of the tube. The bow shock wave shows up between the Mach disk and the tube flow interface most clearly in the last three images. While the dominant mechanism responsible for the jet-screech mode is the oscillating bow shock wave, the tube still swallows and discharges the jet flow at a harmonic of the tube fundamental frequency. This can be seen in the images as the shock wave traverses the nozzle-to-tube gap. Inspection of the pressure-time data reveals a peak-to-peak pressure amplitude of approximately 40 psi. Comparison of this data with that of the previous case at X = 0.4-inch in Figure 9, indicates a large increase in frequency associated with the transition from jet-regurgitant to jet-screech and a slight decrease in pressure amplitude. Both the increase in frequency and decrease in pressure amplitude, as the HST transitions from jet-regurgitant to jet-screech mode, are consistent with what was observed in the data at X = 1.0-inch, shown in Figure 8.

The next case, illustrated in Figures 11 and 12, shows data for the HST operating at X = 1.0-inch for R = 15.8. For this case, the tube inlet fluctuating pressure signal, used to trigger the Schlieren system light source, was recorded in addition to the end-wall pressure. The two signals were monitored simultaneously on the digital oscilloscope. Inspection of the two signals, simultaneously displayed on the same time scale, allows observation of the relationship between the two. A screen shot image of the oscilloscope display, at X = 1.0-inch and R = 15.8, is shown on the right in Figure 11.

Examination of the simultaneous fluctuating pressure data reveals that every 2nd peak of the tube inlet pressure coincides with the minimum of the tube end-wall pressure. The other tube inlet pressure peak coincides with the second end-wall pressure peak. This suggests that, at frequencies significantly higher than

the fundamental, the driving frequency is determined by the jet pressure ratio and nozzle-to-tube-gap. However, the response of the tube depends on the tube natural frequency and harmonics. Therefore, the tube inlet pressure yields the driving frequency, which is set up by the interaction between the bow shock wave and tube inlet while the end-wall pressure yields the frequency response of the tube. It is postulated that resonance occurs when the driving frequency is a multiple of the tube natural frequency (resulting in intense end-wall heating). Furthermore, this observation helps explain why it is sufficient to look over only one tube inlet cycle during the flow visualization sequences as the tube inlet flow does not appear to be greatly affected by the flow within the tube.

Figure 12 shows Schlieren images of the flow between the nozzle and tube during operation in jet-screech mode at X = 1.0-inch for R = 15.8. The Schlieren images for this case represent the dynamic interaction during one tube inlet pressure cycle of 140 μs. The bow shock wave can be seen most clearly in the fourth image, at t = 60 μs. The flow in this image sequence is very similar to the imagery at X = 0.7-inch shown in Figure 10 even though the period is longer (140 μs as apposed to 100 μs). The bow shock wave oscillates inside the second shock cell while the tube swallows and discharges the jet flow.

Helium Results

In order to ascertain the effects of gas molecular weight on the HST operation, helium was substituted for air as the working gas. Tests were run to determine the end-wall temperatures as a function of pressure and nozzle-to-tube gap. In the interest of conserving helium, only three gaps for each tube were tested and the range of pressures tested was traversed at a roughly constant rate without allowing the apparatus to entirely reach equilibrium temperature at each collected data point. Traversing the pressure range in both directions and measuring the difference in temperature determined the consequence of the hysteresis on the data. The error was measured to be an approximately ±5% uncertainty in peak temperature.

The results at X = 1.0-inch are shown in Figure 13 along with the data for air at X = 1.0-inch for the purposes of comparison. Comparison of the helium data to the data obtained with air reveals major differences in the temperature trend. Three distinct temperature peaks are present in the air data, while the helium data shows five peaks. Also, the peaks do not occur at the same pressure ratios, with the exception of the second peak in the air data. All of the peak temperatures are higher with helium up to R = 13, where the air data continues to steadily climb in temperature and the helium data drops.

Figure 14 shows data for the HST operating at X = 0.7-inch with air and helium. Comparison of the helium data to the data obtained with air again reveals major differences in the temperature trend at this nozzle-to-tube gap. Two distinct temperature peaks are present in the air data, while the helium data shows three, not so distinct peaks. Also, the last temperature peak does not occur at the same pressure ratio and all of the peak temperatures are higher with helium.

The results at X = 0.4-inch are shown in Figure 15 along with the data for air at X = 0.4-inch. Comparison of the helium data to the data obtained with air reveals major differences in the temperature trend. Only one small temperature peak is present in the air data, while the helium data shows two large peaks. Also, the peak in the air data does not occur at the same pressure ratio as either of the two helium peaks. The temperatures are much higher with helium than air.

In summary, each gap case studied for the helium data appears to have a unique trend; in contrast to the air data where all gaps studied had similar relationships in pressure and temperature. Additionally, the maximum peak temperature ratio for helium was higher at T/T_a = 2.8 for the data taken at X = 0.7-inch than air at T/T_a = 2.6 for the data taken at X = 1.0-inch.

In order to gain an understanding into the flow mechanisms involved in creating the five temperature peaks for the 1.0-inch gap, an in-depth investigation of this case was conducted. The end-wall fluctuating pressure at each of the five temperature peaks was obtained using the PCB pressure transducer. The results of the study are shown in Figure 16. Schlieren imagery is not reported as the large density gradients due to the interaction of the helium and laboratory air make it difficult to obtain the dynamic flow visualization.

Without the advantage of flow visualization, it is useful to compare the data available with the data in Figure 8, where flow visualization is available and the modes are more easily identified. The data for the case of R=2.7, at the top of Figure 16, indicates that the jet-regurgitant mode is excited. This is evident in both the fluctuating pressure waveform and frequency domain data. Comparison of the helium data waveform with the waveform of the air data, for the jet-regurgitant mode, yields similarity as both are of the "shock-type" wave. Furthermore, the FFT data for helium indicates a fundamental frequency of f = 6.8 kHz which agrees well with the calculated value from the fundamental tube frequency equation of f = 6 kHz.

The data from the next two cases, at R = 4.4 and R = 5.4, indicates that the HST is operating in the jet-screech mode. Again, both comparison of the fluctuating pressure waveforms with the air data and the high frequency fluctuations indicated in the power spectral density plot support this conclusion. Also, the waveform has transitioned to the sinusoidal-type wave.

The last two cases, for R = 8.7 and R = 16.0, are difficult to identify. The waveform appears to have transitioned back to the "shock-type" wave that is often

observed in the jet-regurgitant mode. Inspection of the FFT data reveals peaks at f = 10.7 kHz and f = 7.8 kHz for the R = 8.7 and R = 16.0 cases respectively. The calculated fundamental tube frequencies, using the respective end-wall temperatures for each case, are f = 8.6 kHz and f = 8.3 kHz. Both the similarity in these waveforms with those for the jet-regurgitant mode and the low frequency harmonics in the FFT data appear to indicate that the jet-regurgitant, not the jet-screech, mode is excited. This conclusion is contradictory to what was observed in the air data and difficult to substantiate without additional data including flow visualization.

Overall, the HST produced higher (on average, approximately 25%) end-wall temperatures with helium than with air. However, the optimum operating pressures are different for the two gases. These results differ from those reported by Phillips and Pavli where approximately 75% higher end-wall temperatures were obtained at the same operating parameters.

Comparison of the fluctuating pressure data at the first three temperature peaks with helium at X = 1.0-inch which occur for R = 2.7, 4.4, and 5.4 with data at the three temperature peaks with air, which occur at X = 1.0-inch for R = 2.3, 4.7, and 15.8, reveals that higher end-wall pressure frequencies are encountered with helium in these particular cases.

It is important to note that the helium cases were run in a laboratory environment where air surrounds the apparatus. The helium nozzle jet impinges on the tube through the laboratory air as opposed to a pure experiment where a helium jet impinges on the tube in a closed environment of helium. The consequences of this are: (1) the actual gas composition at the nozzle-to-tube interaction is composed of both helium and air and, (2) as the experiment is run, helium begins to flood the laboratory, possibly making the experiment time-dependent and unrepeatable.

In order to determine the effects of the two different gases used in this experiment, several key issues must be examined. The molecular weight of the working gas should not affect the dimensionless frequencies and shock angles. Thus, running the experiment with any gas of a consistent molecular weight would not be expected to affect the temperature performance of the HST. Therefore, two things can be responsible for the changes in the temperature performance for the two different working gases used: (1) the different specific heat ratios or, (2) the coupling of the outwardly moving tube flow with the surrounding gases (of different molecular weight and specific heat ratio). Since a change in specific heat ratio generally does not usually greatly influence flow characteristics, it is speculated that the differences between the helium and air results in this experiment are due to the coupling and its feedback effects on the flow in the apparatus.

Open-Tube Performance

The next step in evaluating the HST was to determine the open-tube performance and the relationship between the amount of gas extracted and end-wall temperature. With the HST in the second configuration, data was acquired. The HST was tested at the pressure ratios corresponding to the highest peak temperature for each of the three nozzle-to-tube gaps studied, X = 0.4, 0.7, and 1.0-inch, for a total of three cases using air. An additional case using helium was studied as well at X = 0.7-inch. The experimental data obtained for extracted-gas flow rate and end-wall temperature is presented in Figure 17. Both the air and helium cases performed similarly. The trend is a significant drop in end-wall temperature as the extracted-gas flow rate increases. The end-wall to ambient temperature ratio falls below a factor of two well before the extracted-gas flow rate reaches one tenth of one percent of the nozzle flow. While the helium cases resulted in slightly higher extraction rates, the HST still does not produce significant extraction flow rates without a drastic reduction in performance.

It was speculated that the highest end-wall temperatures are reached at different pressure ratios when the HST is in the open configuration than when in the closed configuration. Therefore, an investigation was conducted in order to ensure that the HST was still in the optimum configuration during extraction. With the apparatus configured for extraction, the inlet pressure was varied from 0-425 psig while measuring the end-wall temperature. This was done at a constant extraction flow rate of approximately 12 SLPM. A nozzle-to-tube gap of X = 1.0-inch was used for this experiment because this case has the most experimental data, including flow visualization.

Comparing the data during extraction, in Figure 18, with the data in the closed-end configuration (0 SLPM), repeated here for comparison, reveals that extracting gas does not significantly alter the pressures where the end-wall temperature is at a minimum. The temperature maxima at X = 1.0-inch occur at nozzle-to-ambient pressure ratios of approximately R = 2.5, 4.0, and 15.8 regardless of whether gas is extracted from the tube.

CONCLUSIONS

A Hartmann-Sprenger Tube has been developed to explore the heating phenomenon at the end-wall of the cavity. Schlieren flow visualization of the nozzle-to-cavity interaction was used and dynamic pressure traces at the cavity end-wall were investigated to ascertain the differences in operating modes and their effect on heating performance. The results agree well with current theory and previous research.

With the HST in the closed-end configuration, the end-wall temperature was determined as a function of nozzle pressure and nozzle-to-cavity gap distance for

the HST. The largest end-wall to ambient temperature ratio recorded was T/Ta = 2.6 at R = 15.8.

Schlieren imagery of the nozzle-to-cavity interaction and dynamic pressure at the end-wall was investigated. The HST was investigated at three separate nozzle-to-cavity gaps. A total of three cases were tested, each at the pressure corresponding to the largest end-wall temperature produced. The respective operating modes were identified from the flow visualization, dynamic pressure time-domain data, and dynamic pressure frequency-domain data. The HST was observed to operate with dominant end-wall pressure frequencies of up to 27 kHz while in jet-screech mode and fluctuating pressure amplitudes of up to 3.7 atm.

In addition to Air, Helium was used as the working gas in the HST in order to ascertain the effects of different gas compositions on the performance of the apparatus. An increase in end-wall temperature of approximately twenty-five percent was achieved, on average, with Helium verses Air.

An investigation was conducted of the effects of extracting gas from the end of the cavity. The tests were performed with both Air and Helium. A reduction in the end-wall to ambient temperature ratio to below a factor of two occurred at extraction flows lower than one percent of the nozzle flow, indicating a strong disturbance in the flow phenomenon inside the cavity.

In conclusion, a working Hartmann-Sprenger Tube has been developed. The objective of ascertaining the characteristics of the different modes of operation and their effect on heating performance was met. The effects of using a lighter gas on the performance of the HST were explored. Finally, gas was extracted from the end-wall of the tube to determine the end-wall temperature as a function of the gas extraction flow rate.

ACKNOWLEDGEMENTS

The authors would like to acknowledge the support of the Hypersonic Airbreathing Propulsion Branch at NASA Langley Research Center.

REFERENCES

[1] Hartmann, J., and Troll, B., "On the New Method for the Generation of Sound Waves," *Physical Review*, Vol. 20, 1922, pp. 719-727.

[2] Sprenger, H.S., "On Thermal Effects in Resonance Tubes," *Mitt. Eidgnedoss. Tech. Hoch. Inst. Aerodynamik,* Zurich, No. 21, 1954, pp. 18-35.

[3] Sarohia, V., and Back, L.H., "Experimental Investingation of Flow and Heating in a Resonance Tube," J. Fluid Mech.,Vol. 94, Part 4, 1979, pp 649-672.

[4] Powell, A., "On the noise emanating from a two-dimensional jet above the critical pressure," *Aeronautical Quarterly*, Vol. IV, 1953, pp 103-122.

[5] Phillips, B.R., and Pavli, A.J., "Resonance Tube Ignition of Hydrogen-Oxygen Mixtures," NASA Technical Note TN D6354, May 1971.

[6] Kreutz, T.G., and Law, C.K., "Ignition in Nonpremixed Counterflowing Hydrogen Versus Heated Air: Computational Study with Skeletal and Reduced Chemistry," *Combustion and Flame,* Vol. 114, 1998, pp. 436-456.

[7] Bouch, D.J., "Development and Investigation of a Hartmann-Srenger Tube for Passive Heating of Scramjet Injectant Gases," Master's Thesis, Dept. of Mechanical and Aerospace Eng., The George Washington Univ., 2002.

[8] McAlevy , R. F., and Pavlak, A., "Tapered Resonance Tubes: Some Experiments," AIAA, Vol. 8, No. 3, Mar. 1970, pp. 571-572.

[9] Bendat, J.S., and Piersol, A.G., "Random Data: Analysis and Measurement Procedures," *Digital Data Analysis Procedures,* Wiley-Interscience, New York, 1971, pp.324-327.

[10] Kang, S., "Resonance Tubes," Ph.D Thesis, Dept. of Mech. Eng., Rensselear Polytechnic Inst., 1964.

FIGURES

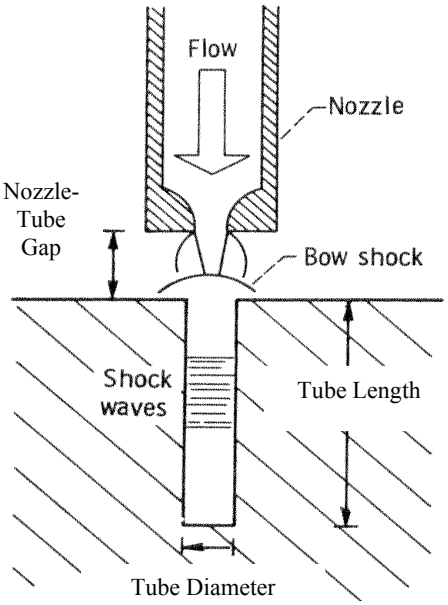

Figure 1 – Basic Hartmann-Sprenger Tube Configuration (Phillips and Pavli)

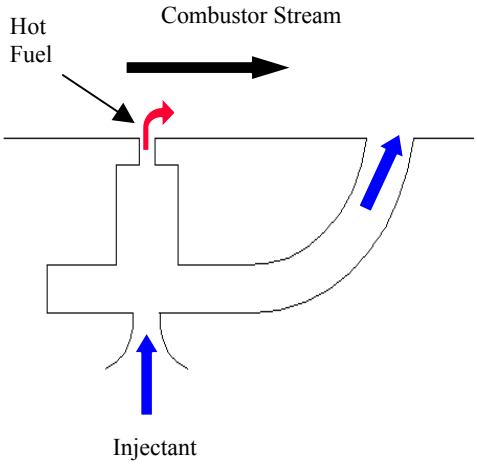

Figure 3 - Proposed Configuration for Scramjet Piloting

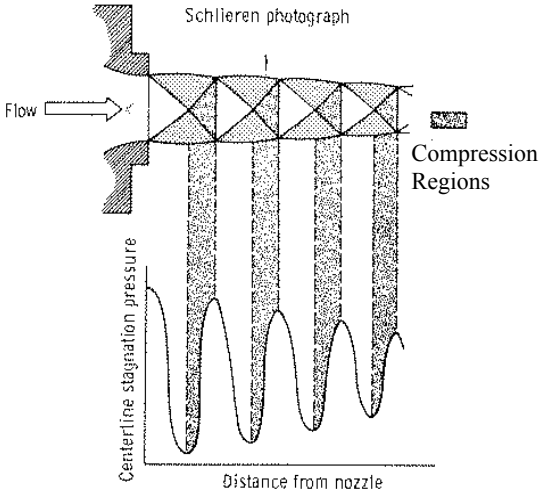

Figure 2 – Jet Shock Cell Structure and Regions of Compression (Phillips and Pavli)

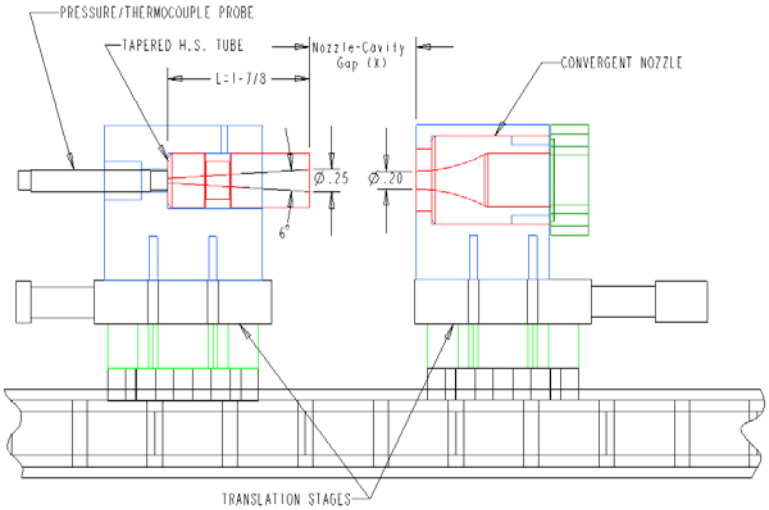

Figure 4 – Hartmann-Sprenger Tube Component Layout

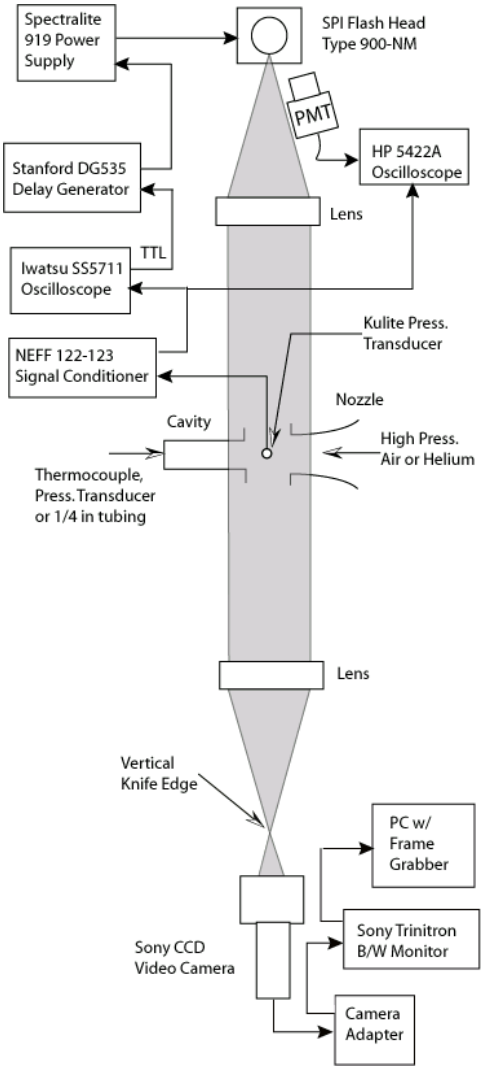

Figure 5 – Instrumentation and Schlieren System Layout

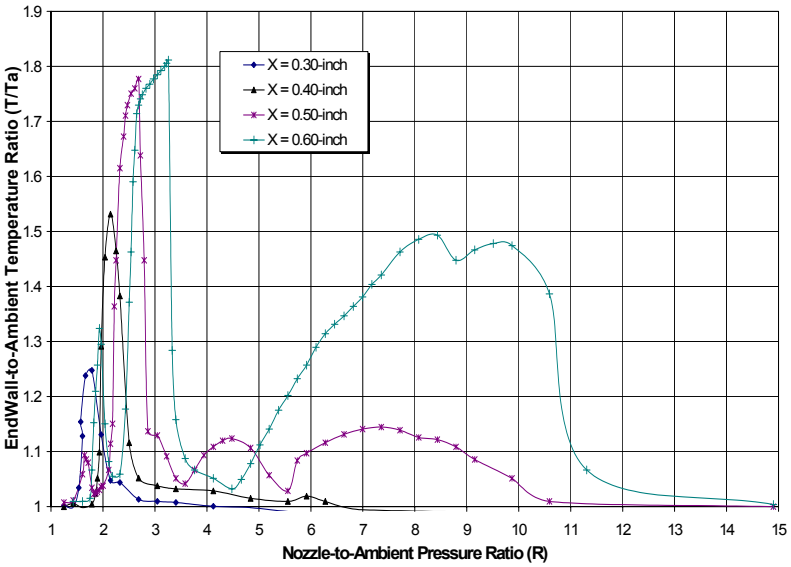

Figure 6 –Hartmann-Sprenger Tube Closed-End Air Performance (Small Gaps)

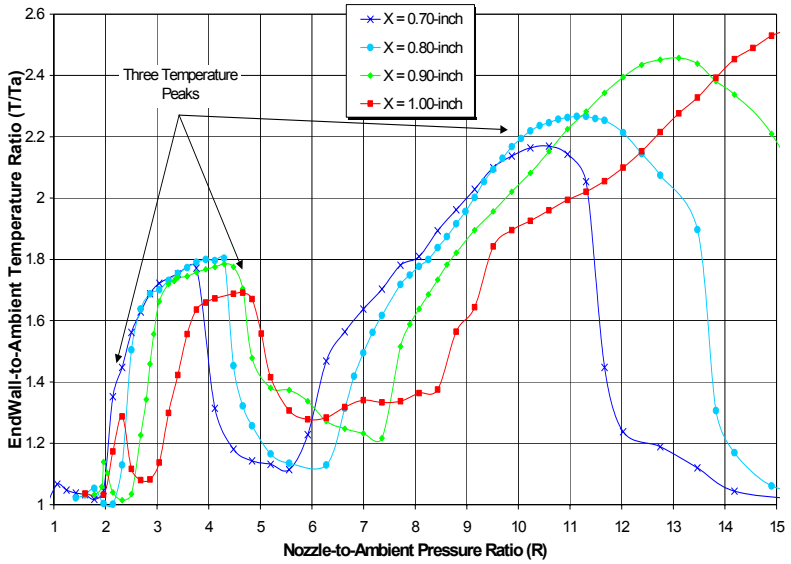

Figure 7 - Hartmann-Sprenger Tube Closed-End Air Performance (Large Gaps)

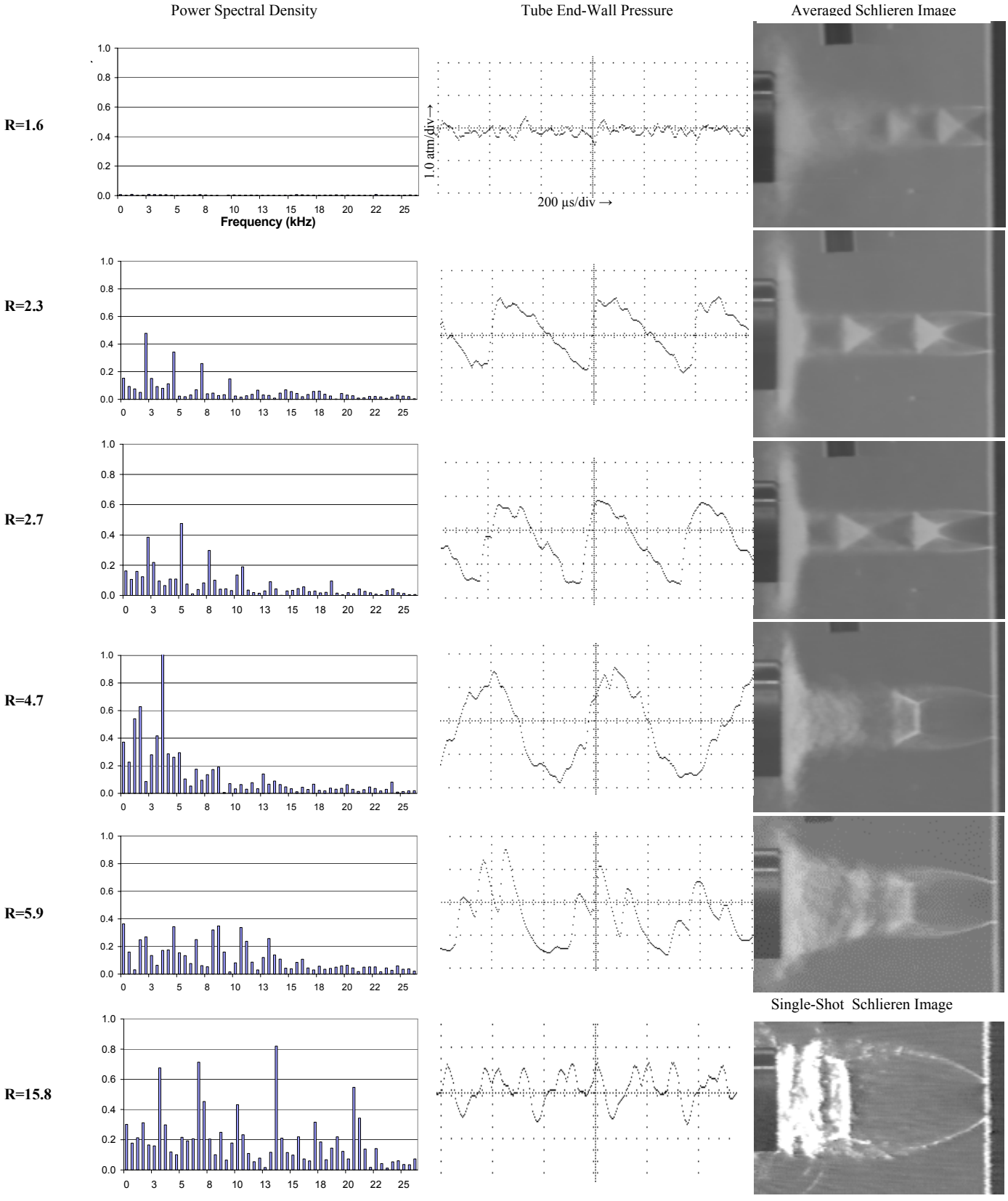

Figure 8 – End-Wall Pressure and Flow Visualization at X=1.0-inch

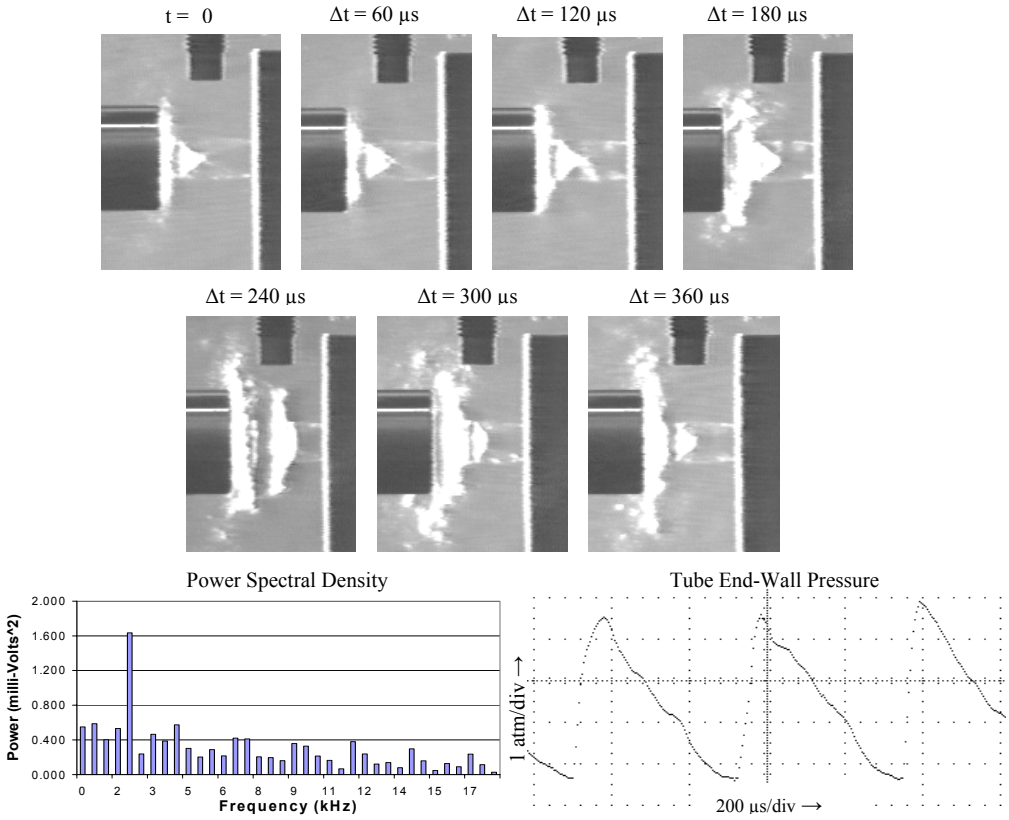

Figure 9 – Hartmann-Sprenger Tube Operating at X=0.4-inch and for R=2.1

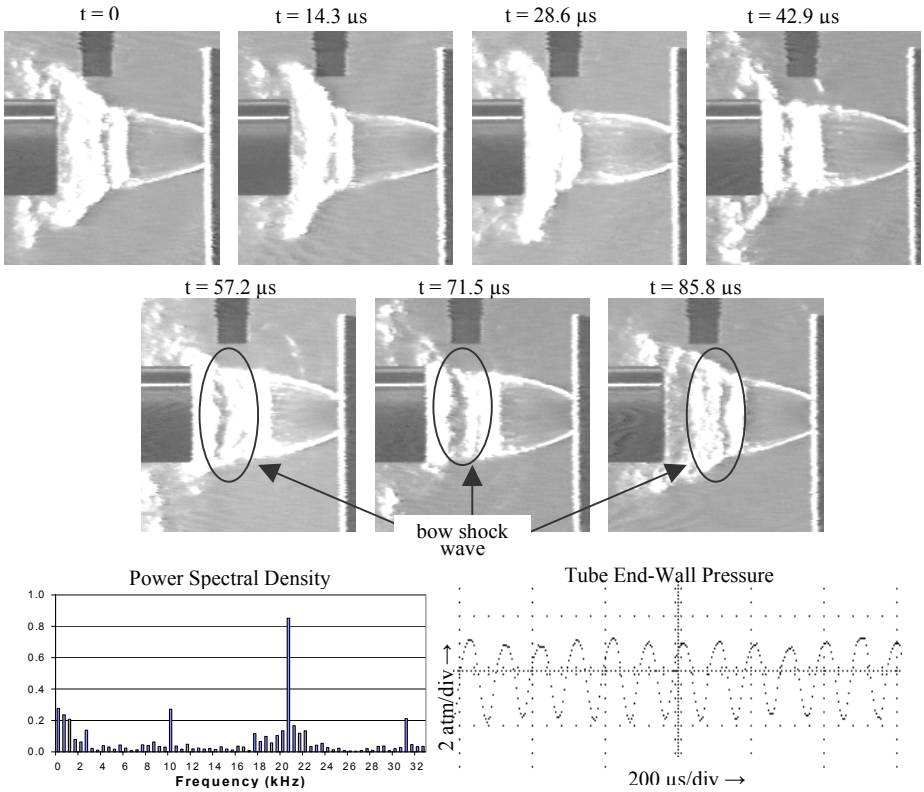

Figure 10 – Hartmann-Sprenger Tube Operating at X=0.7-inch and for R=10.4

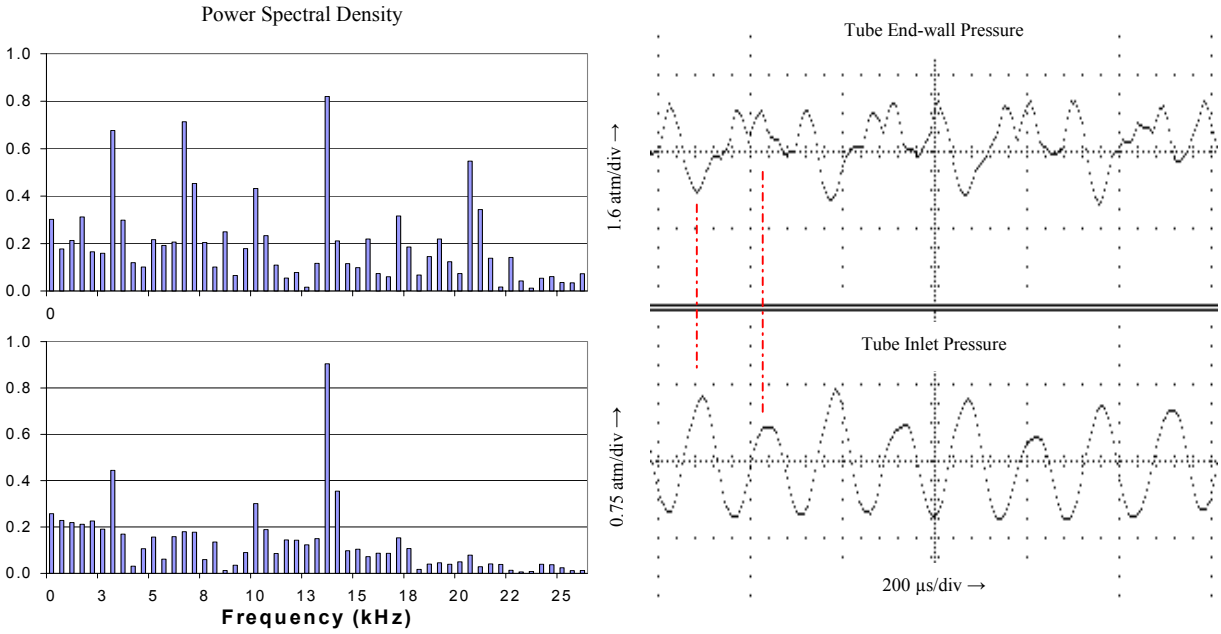

Figure 11 – Time-dependent Pressure in the Hartmann-Sprenger Tube Operating at X=1.0-inch and for R=15.8

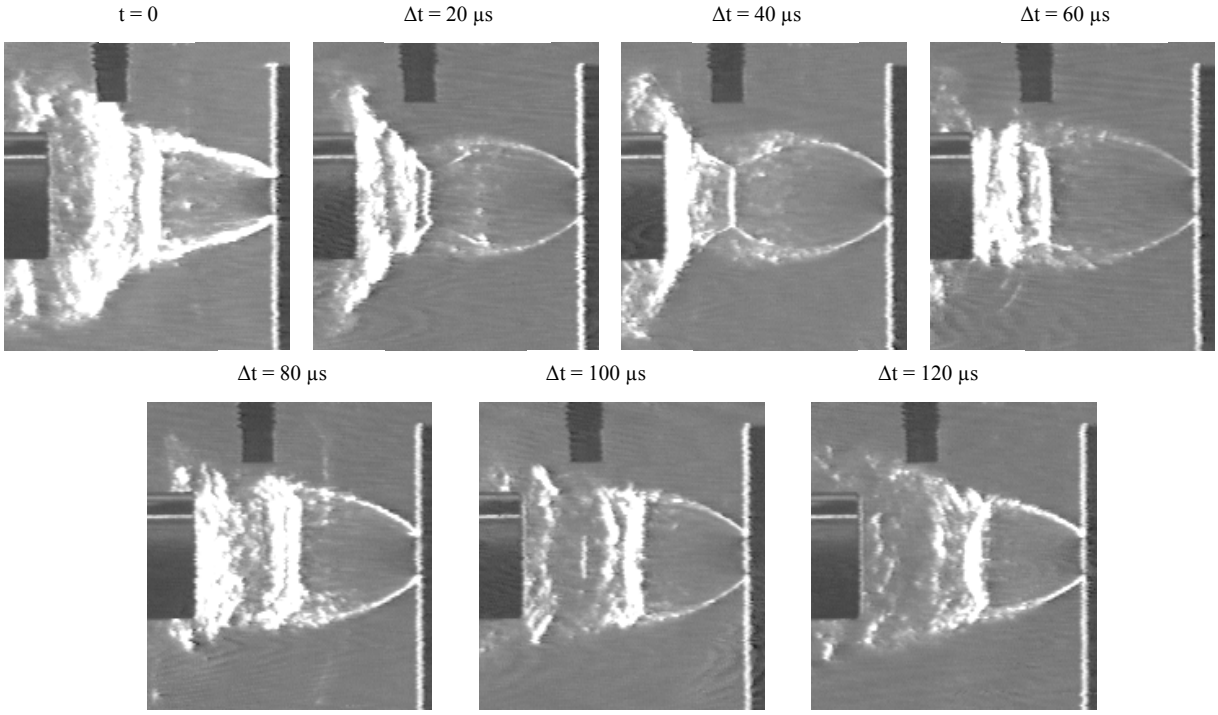

Figure 12 – Schlieren Image Sequence of the Hartmann-Sprenger Tube Operating at X=1.0-inch and for R=15.8

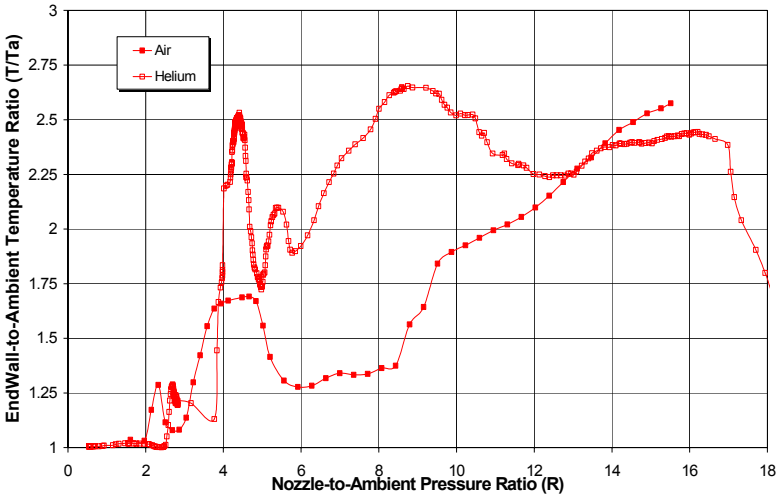

Figure 13 – Hartmann-Sprenger Tube Closed-End Helium Performance (X = 1.0-inch)

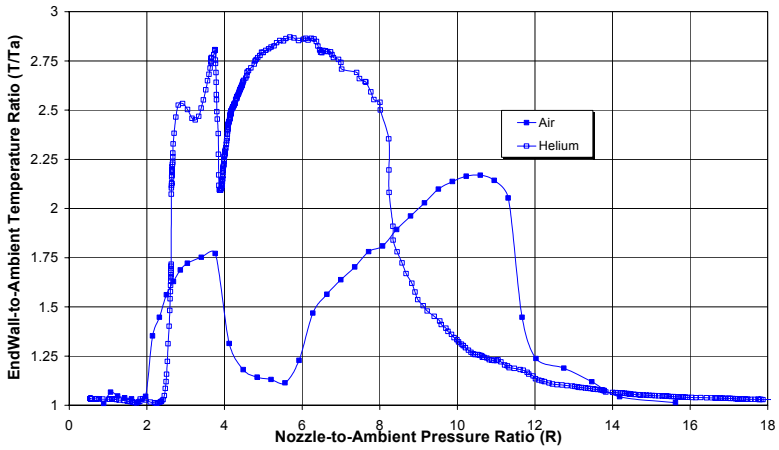

Figure 14 – Hartmann-Sprenger Tube Closed-End Helium Performance (X = 0.7-inch)

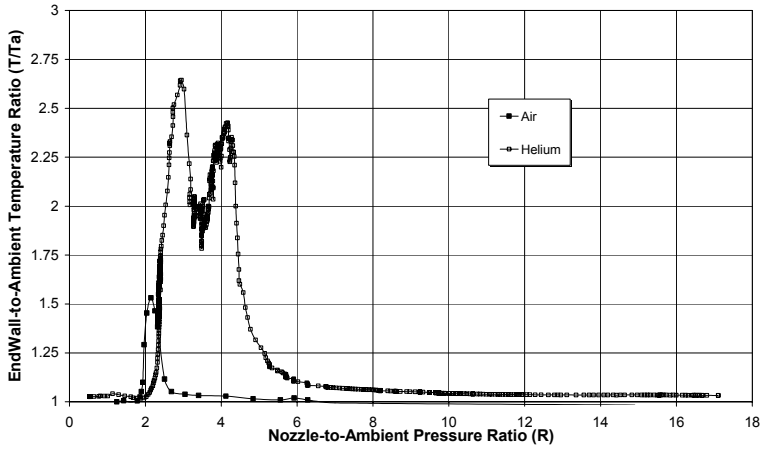

Figure 15 – Hartmann-Sprenger Tube Closed-End Helium Performance (*X* = 0.4-inch)

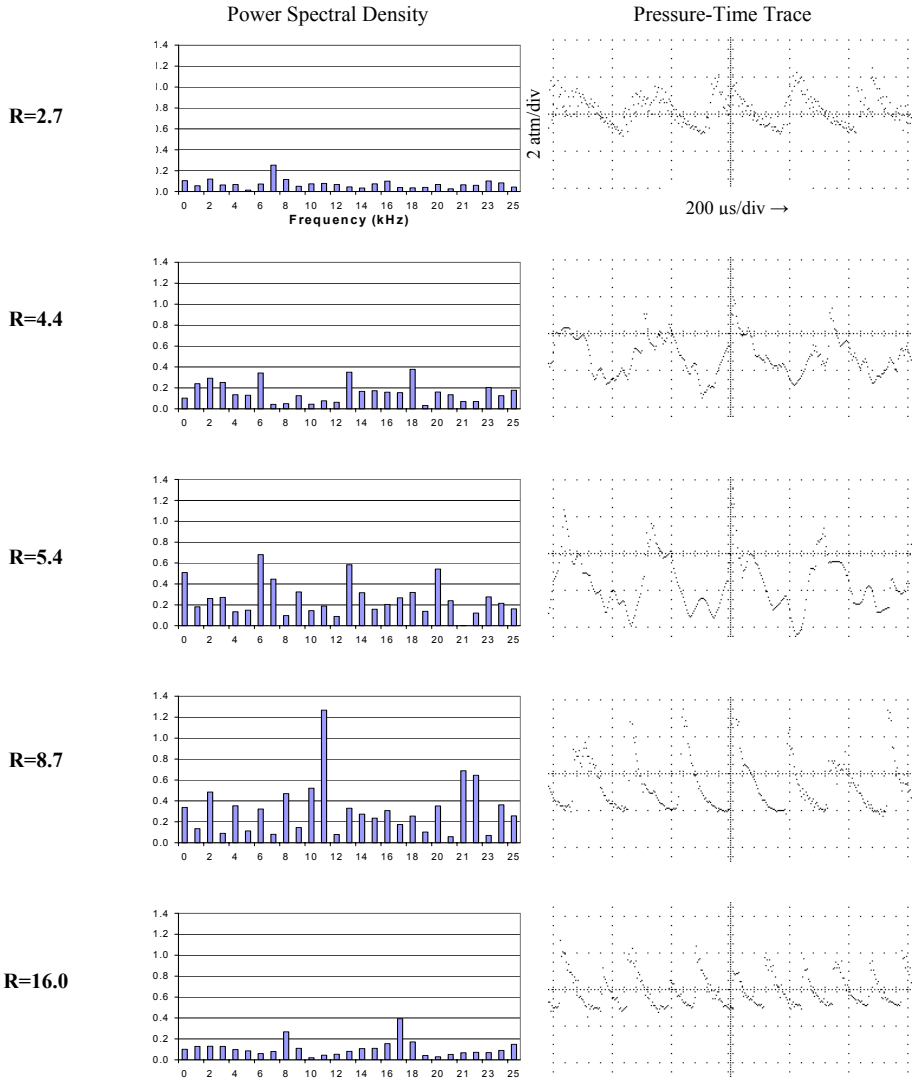

Figure 16 – End-Wall Pressure at 1.0-inch Gap and Selected Nozzle Pressure Ratios for Helium

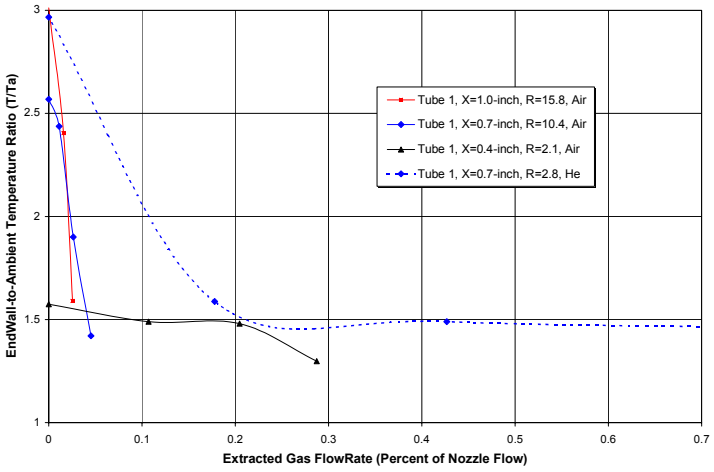

Figure 17 – Gas Extraction Performance

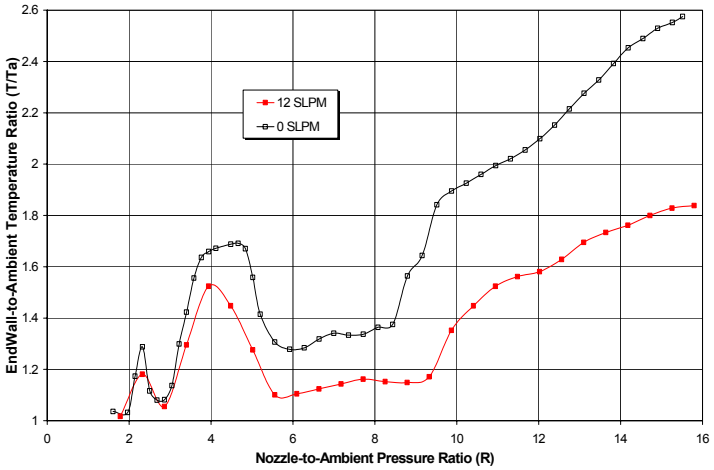

Figure 18 – Extraction Performance at X = 1.0-inch